Independent production cross sections for Hg isotopes from the reaction of 600-MeV ^{18}O with Pb

Zhang Li,* Zheng Jiwen, Zhao Jinhua, Yang Yongfeng, Qin Zhi, Hu Qingyuan, Zhang Chun, Wang Jicheng, and Wei Hao
Institute of Modern Physics, Chinese Academy of Sciences, Lanzhou 730000, People's Republic of China
(Received 12 July 2001; revised manuscript received 14 April 2004; published 25 August 2004)

Independent cross sections for all the Hg isotopes produced in the reaction of 600-MeV ^{18}O with a molten natural Pb target have been measured down to about 2 μb. The measurement is based on a radiochemical gamma-spectroscopy technique combined with rapid gas thermochromatography. The observed Hg-isotope distribution from ^{180}Hg to ^{209}Hg is compared with those previously reported from the reaction of 600-MeV p with a natural Pb target, and from two-proton-removal reactions measured by the inverse-kinematics method at relativistic energies. The comparisons make available some additional information for improving knowledge of spallation-reaction mechanisms in peripheral nuclear collisions. It is noted that the production cross sections for neutron-deficient heavy residues and the yield of fast neutrons emitted in proton-induced reactions should increase with increasing incident proton energy from 600 MeV to 1 GeV.

DOI: 10.1103/PhysRevC.70.024603 PACS number(s): 25.70.Mn., 24.10.-i, 25.40.Sc, 29.25.Dz

I. INTRODUCTION

Precision measurement of the distribution of heavy projectile residues from spallation reactions induced by projectiles such as Pb and U at relativistic energies seems increasingly important in view of recent progress in heavy-ion reaction studies. First, there is considerable demand for reliable data on varieties and their yields as well as the kinetic energies of neutrons emitted in such a collision process. These data are especially important in designing a fast neutron source for accelerator-driven subcritical reactors [1] or spallation neutron sources [2]. Second, precision measurements will provide a tool to study the excitation mechanism of heavy-ion nuclear reactions at relativistic energies, and to examine theoretical models that describe relativistic nuclear reaction processes and predict yields of the various products.

So far most experiments have been conducted on the fragment separator (FRS) at GSI by means of a physical identification technique based on kinematic analysis and ion-optical separation as described in Refs. [3–10]. The FRS enables isotopes produced in spallation reactions to be simultaneously separated and identified [11]. Thus one can evaluate independent cross sections for isotopes produced down to 0.1 mb. To make use of them in designing such a neutron source these data should be converted into those for high-energy neutron- or proton-induced reactions using the inverse-kinematic principle. Needless to say, the knowledge of target residues produced in bombarding heavy targets, such as lead, bismuth, and mercury, with high-energy neutrons or protons would be very practical for that purpose. It seems, however, that there are rich varieties in energetic heavy-ion-induced reactions which are still useful in understanding high-energy neutron-or proton-induced reactions with the inverse-kinematic principle.

A number of measurements have been reported of independent cross sections for heavy residues using spectroscopic techniques [12–14], but most of the measurements were obtained from cumulative yields after a long decay chain except for a few cases. The cross sections reported are limited to about 1 mb.

In this paper we shall describe a successful attempt to evaluate independent production cross sections for Hg isotopes in the 600-MeV ^{18}O+Pb reaction by means of a radiochemical γ-spectroscopic technique. Measurements have successfully been made down to 2 μb. The measured Hg-isotope distribution provides information about the dependence of yields and distributions of the residues on the projectiles and their energies. Comparison is made between previously available data and the present data.

II. EXPERIMENT

A 600-MeV ^{18}O beam was provided from an intermediate energy heavy-ion accelerator at the Heavy Ion Research Facility at Lanzhou (HIRFL) Institute of Modern Physics to irradiate a molten natural lead target with a thickness of about 5.2 g/cm^2 (thick enough to stop the 600-MeV ^{18}O incident beam). The average beam was 2.2 pnA.

An on-line gas thermochromatographic separation device combined with a running-rabbit system has been developed as described previously [15,16]. This device enables a series of operations to be automatically made at a preset schedule: controlling the irradiation time, monitoring the beam current, separating elements from the target, transmitting the collected elements at the exit of the chromatography tube to a low-background γ-ray measurement station within 20 s, and setting a new catcher foil at the exit of the tube where a vacuum of about 10^{-2} Pa is usually maintained. The temperature of the molten lead target material was continuously kept at about 700 °C during the ^{18}O beam irradiation. The maximum escape depth of reaction products from the molten lead target material was limited to 4.4 mm due to the specially designed step-form graphite target box used [15]. Therefore, the release time was much shorter than 5 s for volatilizable element products such as Hg isotopes. Volatile reaction products such as Hg, Tl, At, and Po from the lead target were transferred and separated by means of the on-line

*Email address: zhangli@impcas.ac.cn

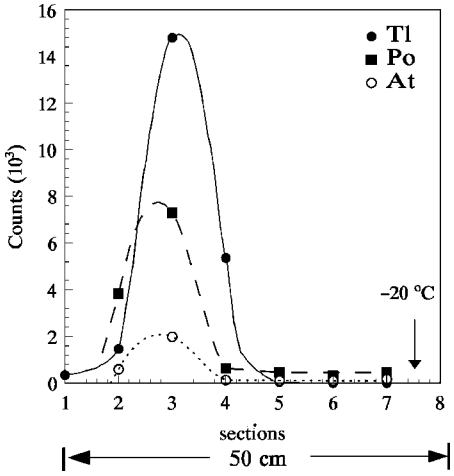

FIG. 1. Element distribution of the volatile products deposited along the transfer tube in the present gas thermochromatography. 1–6 denote different sections along the transfer tube.

gas thermochromatographic setup and collected into a catcher foil positioned at the exit of the tube. In the present work we used a set of gold-foil catchers and collected Hg isotopes, which were well separated from other reaction products. The temperature gradient along the tube is from about 700 °C at the entrance to about −20 °C at the exit. The transmission time from the target surface to the exit of the tube, i.e., the position of the catcher foil, was not longer than 1 s. To identify the elements along the tube, we conducted a test irradiation of the lead target with a 600-MeV ^{18}O beam for 100 min and measured γ rays from different sections of the tube as indicated in Fig. 1.

The Hg collection efficiency of the present setup was measured to be $(85\pm10\%)$ by making use of a ^{203}Hg-isotope label technique. The label isotope ^{203}Hg was produced by irradiating natural lead pieces with 14-MeV neutrons: the neutron flux was about 2×10^{11}/s cm^2 and the irradiation duration about 70 h. The irradiated lead pieces were cooled down for two months or more. We measured the intensity of the 279-keV γ rays from ^{203}Hg produced in one of the irradiated lead pieces for reference and cut that piece into parts as tiny as possible to place at the target position in the gas thermochromatographic setup. The sample at the target position was heated up to about 700 °C to vaporize ^{203}Hg so that it was collected on a gold-foil catcher at the exit of the setup. The ratio of the 279-keV γ-ray intensity from the original lead piece to that from the gold foil gives the Hg collection efficiency. We repeated this procedure eight times to get the efficiency accurately enough for the present purpose.

The detector system at the low-background γ-ray measurement station consists of a *p*-type high-purity (HPGe) detector (full width at half maximum 1.9 keV at 1332.5 keV γ-ray energy), a large bismuth germanate detector ($14\times7\times5$ cm^3) and a β-ray detector, which enable us to make $4\pi\Delta E_\beta$-E_γ coincidences with veto signals from β^+ decays. The detection efficiency of the HPGe detector was calibrated with a standard ^{152}Eu gamma source. Details have been described in Refs. [15,17]. The Compton background was reduced to about one-tenth, which enabled weak γ rays from neutron-rich Hg isotopes to be detected with a high efficiency of $(46\pm3)\%$ relative to the corresponding single γ-ray spectra.

To evaluate individually the independent cross sections for Hg-isotope production in the 600-MeV ^{18}O+^{nat}Pb reaction, three different irradiation-detection periods were employed: first, the cycle was a 120-s irradiation followed a 420-s γ-ray detection, and a total of 143 samples were measured; second, 10-min irradiation followed by 60-min detection and three samples; third, 100-min irradiation followed by 48-h detection for one sample.

III. DATA ANALYSIS AND RESULTS

To evaluate independent cross sections for Hg isotopes, special care has been exercised over the following difficulties: (1) half-lives of some Hg isotopes are very short in comparison with the time elapsed before starting the measurement (typically 20 s after irradiation); (2) for some Hg isotopes γ-decay schemes and/or absolute γ-ray branching ratios have not been measured; (3) γ rays which should be characteristic of some Hg isotopes including relevant daughter or granddaughter nuclides are too weak to be identified or overlapping with other γ rays.

Starting with the primary product concerned, we identified γ rays characteristic of all nuclides in its long decay chain and observed the decay curve. To estimate the numbers of atoms of nuclides from generation to generation, the analysis was made in the following way, details of which were described in Ref. [18]. Mention should be made of the fact that our method is valid only for the case that the primary collected product is restricted to the isotopes of a single separated element.

During target irradiation, the number of atoms of the Ith generation $N_I(t)$ at time t is given by

$$N_I(t)=\frac{M}{\lambda_I}\left(1+(-1)^I\sum_{i=1}^{I}e^{-\lambda_i t}\prod_{\substack{j\neq i\\ j=1}}^{I}\frac{\lambda_j}{\lambda_i-\lambda_j}\right),$$

where $I=1$ denotes the primary isotope concerned, λ_I the decay constant of the Ith generation nuclide, and M the production rate of the primary isotope. Obviously, $M=I_B n_A\sigma$, where I_B is the number of incident ions per second, n_A the effective target thickness (0.67 g/cm^2) in numbers of atoms per square centimeter corresponding to the projectile energy loss from the incident energy (600 MeV) down to the interaction Coulomb barrier (about 86 MeV), and σ the isotope production cross section averaged over the effective range of interaction energy.

After irradiation, the number of atoms of the Ith generation nuclide $N_I^d(t_d)$ is given by

$$N_I^d(t_d)=\sum_{k=1}^{I}(-1)^{I-k}\left(\prod_{i=k}^{I-1}\lambda_i\right)N_k^0\times\left[\sum_{i=k}^{I}e^{-\lambda_i t_d}\Big/\prod_{\substack{j\neq i\\ j=k}}^{I}(\lambda_i-\lambda_j)\right],$$

where t_d is the time since irradiation stopped. The amount

$N_I^d(t_d)$ is experimentally determined by measuring yields of one or several γ rays characteristic of the Ith generation isotope, and its primary number of atoms $N_I^0(t_d)$ at $t_d=0$ is deduced. At the end of the irradiation time $t=t_a$, $N_I(t_a)=N_I^0(t_d)$, from which the production cross section σ is calculated.

To evaluate the cross sections for neutron-deficient Hg isotopes, the characteristic γ rays were selected in the chain from the first to the fifth generation, i.e., the primary Hg isotope and isotopes successively produced in the β^+ decay chain such as Au, Pt, Ir, and Os. For the neutron-rich side, use was made of γ rays characteristic of Hg and Tl isotopes. For some Hg isotopes whose ground state and isomeric state were populated simultaneously, the production cross sections were evaluated for both states and the final production cross sections for those isotopes were given by the sum of the cross sections for both states. Cross examinations were made when two to three characteristic γ rays were available.

In Table I the measured independent production cross sections for the radioactive Hg isotopes from the reaction system of 600-MeV ^{18}O with a thick, natural Pb target are listed along with the γ rays which were used in the corresponding cross-section extraction.

Measurement errors of the experimental cross sections are estimated to be 15% to 30%, including the systematic error from collection efficiency determination, statistical error of γ-ray counts, and count contamination to the characteristic γ ray used in cross-section calculation from neighboring γ rays. A probable additional error would come from the uncertainty of the data for γ-ray branching ratio quoted from Ref. [19]. A probable example is the unusual lower measurement cross section for ^{193}Hg as seen in Fig. 2 and Table I, which has not been clarified clear so far.

IV. DISCUSSION

The investigation of Hg isotopes as heavy residues from a nuclear reaction using a lead-element target or a single lead-isotope projectile has typical and significant importance for understanding the nuclear interaction process usually called a peripheral nuclear collision. In addition, the data concerning lead element gain additional importance since in most accelerator-driven system concepts actually discussed, lead or lead-bismuth alloy is considered to be the preferred material of the spallation target.

Figure 2 shows a comparison between the data (closed circles, hereafter denoted by D1) from the European Organization for Nuclear Research (CERN) and the present data (open circles, hereafter denoted by D2) on the mass distribution of Hg-isotope production: the distribution D1 was measured using an on-line isotope mass separator at CERN for the 600-MeV $p+^{nat}$Pb (170 g/cm^2) reaction where the effective interaction energy ranged from 600 MeV to 340 MeV [20]; and the distribution D2 for the 600-MeV ^{18}O$+^{nat}$Pb (0.67 g/cm^2) reaction where the effective interaction energy ranged from 600 MeV to 86 MeV. The two distributions are remarkably similar to each other although the average interaction energy for the distribution D1 is higher than that for the distribution D2. It should, however, be pointed out that

TABLE I. The average cross sections for Hg isotopes produced in the 600-MeV ^{18}O$+^{nat}$Pb (0.67 g/cm^2) reaction.

Mass number A	Half-life $T_{1/2}$	Characteristic γ ray (keV)	Cross section (μb)
180	3.0 s	^{180}Re 902.8	17±54
181	3.6 s	^{181}Ir 107.6	55±14
		^{181}Re 365.5	
182	10.8 s	^{182}Au 154.9	38±18
		^{182}Ir 127.1	
183	9.4 s	^{183g}Os 381.8	36±11
		^{183m}Os 1102.0	32±9.7
184	30.6 s	^{184}Hg 156.0	82±16
		^{184}Hg 236.2	
		^{184}Au 163.2	
185	49.1 s	^{185}Ir 1828.8	134±27
186	1.38 min	^{186}Hg 111.9	235±35
		^{186}Hg 227.8	232±37
		^{186g}Ir 434.8	161±32
		^{186m}Ir 987.0	93±19
187	2.4 min	^{187}Pt 709.2	277±50
187m	1.93 min		
188	3.25 min	^{188}Hg 190.0	541±81
		^{188}Au 266.0	
189	7.6 min	^{189m}Au 166.7	166±20
189m	8.6 min	^{189m}Au 166.7	449±72
190	20 min	^{190}Hg 142.7	948±142
		^{190}Hg 171.5	1017±150
		^{190}Au 301.8	758±136
		^{190}Au 296	704±127
191	49 min	^{191g}Au 277.9	542±95
		^{191g}Au 284.1	
191m	50.8 min	^{191m}Hg 578.8	584±80
192	4.85 h	^{192}Hg 274.8	1327±200
		^{192}Hg 306.6	1255±196
		^{192}Au 316.5	1092±273
193	3.80 h	^{193g}Hg 573.3	1357±203
193		^{193gm}Hg 258.0	848±127
195	9.9 h	^{195g}Hg 180.3	1357±203
		^{195g}Hg 779.8	1080±173
195m	41.6 h	^{195m}Hg 560.3	475±70
197	64.1 h	^{197g}Hg 191.1	492±74
197m	23.8 h	^{197m}Hg 133.9	1479±222
199m	49 min	^{199m}Hg 374.1	299±60
		^{199m}Hg 158.4	293±59
203	46.6 d	^{203}Hg 279	852±300
205	5.2 min	^{205}Hg 203.7	460±115
206	8.15 min	^{206}Hg 305.1	81±16
207	2.9 min	^{207}Hg 351.3	15.4±5
208	41 min	^{208}Hg 583.1	5.0±1.8
209	35 s	^{209}Ti 465.1	1.8±0.6
		^{209}Ti 324.0	2.1±0.7

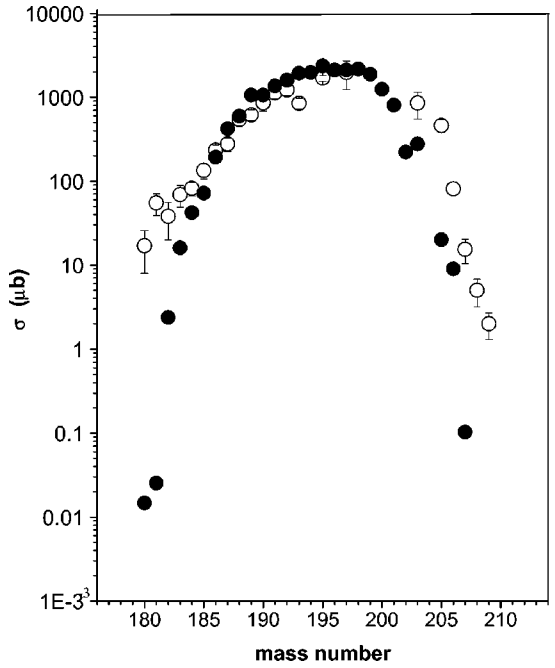

FIG. 2. Experimental Hg-isotopic distributions: closed circles for the 600-MeV $p+^{nat}$Pb (170 g/cm^2) reaction (reproduced from Ref. [18]; open circles for the 600-MeV ^{18}O+^{nat}Pb (0.67 g/cm^2) reaction.

for the distribution D1 the production cross section in the central mass region, i.e., from ^{186}Hg to ^{200}Hg, is slightly larger than that for the distribution D2, which would result from the slightly higher average bombarding energy of the incident proton beam on the lead target.

By using the independent yield distribution of the Hg isotopes measured in the present work, we made a comprehensive intercomparison between the Hg-isotope distributions from two different reaction classes: heavy-ion-induced direct-kinematics reactions at intermediate energies and heavy-ion-induced inverse-kinematics reactions at relativistic energies. For the former, the independent cross-section distributions of the Hg isotopes as targetlike residues, completed in the present work, are the only available data, measured by using a spectroscopic method for the reaction of a 600-MeV ^{18}O beam with a natural lead target; for the latter, three production cross-section distributions of Hg isotopes as projectilelike residues, completed on the FRS at GSI, Darmstadt, were found, corresponding to three different reactions: a 1-GeV/u ^{208}Pb beam with hydrogen [8,9], with deuteron [10], and with copper [5], respectively. If the three reactions are converted into the equivalent direct-kinematics reactions, they correspond to 1-GeV $p+^{208}$Pb, 2-GeV $d+^{208}$Pb, and $\simeq$63-GeV ^{63}Cu+^{208}Pb in order. Figure 3(a) shows the Hg-isotope production-cross-section distribution (circles) from the present work together with the three distributions from the reactions 1-GeV/u ^{208}Pb+p (triangles) [8,9], 1-GeV/u ^{208}Pb+d (full squares) [10], and 1-GeV/u ^{208}Pb +Cu (diamonds) [5]. The four distributions can clearly be divided into two groups. The three distributions in the upper group with higher cross sections correspond to 1-GeV/u ^{208}Pb–induced reactions, and are quite similar to each other

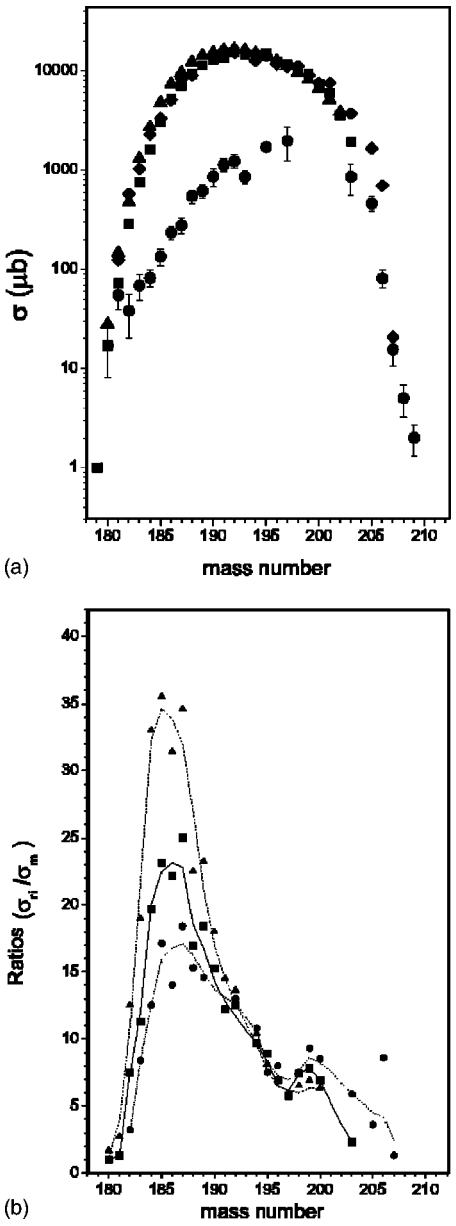

FIG. 3. (a) Production cross sections of Hg isotopes from reactions 600-MeV ^{18}O+^{nat}Pb (circles) (present work); 1-GeV/u ^{208}Pb+p (triangles) [8,9]; 1-GeV/u ^{208}Pb+d (squares) [10]; 1-GeV/u ^{208}Pb+Cu (diamonds) [5]. (b) Ratio curves of Hg-isotope production cross section σ_{ri}, measured for 1-GeV ^{208}Pb projectile induced inverse-kinematic reactions on targets hydrogen ($r=1$), deuteron ($r=2$), and copper ($r=3$), to corresponding cross sections σ_m, measured for 600-MeV ^{18}O+^{nat}Pb reaction (the present work). The lines in (b) were drawn by eye.

in magnitude and shape; the one distribution in the lower group has much lower cross sections and a slowly rising front on the neutron-deficient side, which results from the very thick target used in the present experiment. For most of the neutron-deficient Hg isotopes, the production cross sections in the upper group are, on the average, one order of magnitude higher than that in the lower group. This fact implies that the amount of neutrons emitted from a reaction system will have a huge increase when the bombarding en-

ergy jumps from intermediate energy to relativistic energy.

For the very neutron-deficient Hg isotopes near ^{180}Hg, the production cross sections belonging to the upper group rapidly decrease with decreasing mass number and gradually approach the identical cross-section values of the lower group. This means that the probable maximum number of neutrons evaporated from an excited primary fragment is limited whatever the size of the collision energy. As seen in Fig. 3(a) this number of neutrons is about 26 for two-proton-removal reactions in which Pb nuclei were included as target or projectile. This fact provides a powerful evidence of limit excitation. It is beyond belief that a reaction fragment acquires excitation energy sufficient for the evaporation of up to 26 neutrons by only a very peripheral nuclear collision or a direct two-proton-abrasion process. Therefore, the reaction mechanisms causing many-neutron evaporation should not be the same as those where only a few neutrons are evaporated. There is a real possibility that the very neutron-deficient Hg isotopes may be produced by more central collisions corresponding to smaller collision parameters where proton-neutron evaporation competition would be different from that in very peripheral collisions.

Figure 3(b) shows the cross-section ratio σ_{ri}/σ_m versus Hg-isotope mass number, where σ_{ri} denotes the production cross section of Hg isotopes produced from the 1-GeV/u ^{208}Pb projectile induced reactions. The subscript ri indicates the different targets: hydrogen ($r1$), deuteron ($r2$), and copper ($r3$). σ_m is the production cross section of Hg isotopes from the intermediate-energy heavy-ion nuclear reaction of a 600-MeV ^{18}O beam on a natural lead target (i.e., the present work). Figure 3(b) presents an interesting picture: the ratio curves σ_{r1}/σ_m (triangles and dashed line), σ_{r2}/σ_m (squares and solid line), and σ_{r3}/σ_m (diamonds and dotted line) appear as three obviously distinguishable curves, although the three original Hg-isotope distributions in the upper group are quite similar to each other. Every one of the three curves shows an obvious peak in the neutron-deficient region from ^{183}Hg to ^{193}Hg, where the highest peak is related to the reaction 1-GeV/u ^{208}Pb+p, the middle one to 1-GeV/u ^{208}Pb+d, and the lowest one to 1-GeV/u ^{208}Pb+Cu. With increasing mass number the three curves turn down and gather together in the mass region of 193–196, then separate again from each other, and show a little peak in the neutron-rich region of ^{198}Hg to ^{202}Hg for every curve. However, the curve arrangement from high to low has been reversed in the little peak region, i.e., the order becomes σ_{r3}/σ_m, σ_{r2}/σ_m, σ_{r1}/σ_m. The three distinguishable curves suggest that the three Hg-isotope distributions are specifically different in configuration. Obviously, the ratio of σ_{ri} to σ_m is more sensitive to different reaction systems than the direct isotopic distribution. Every one of the three ratio curves displayed a peak in the very neutron-deficient region and a little peak in the neutron-rich region, which implies that two different reaction mechanisms contributed to the production of the Hg isotopes related to the two-proton-removal process at relativistic energy.

Combining Fig. 3(b) and Fig. 3(a), some useful information about the reaction mechanism can be extracted. Among the three reaction systems the distribution related to the reaction 1-GeV/u ^{208}Pb+p is the most neutron-deficient one with the highest yield of neutron-deficient Hg isotopes as well as the lowest yield of neutron-rich Hg isotopes, compared to the other two reactions. On the contrary, the distribution related to the reaction 1-GeV/u ^{208}Pb+Cu is clearly shifted to the more neutron-rich side, and shows the highest yield of neutron-rich Hg isotopes. A similar case was discovered by Benlliure *et al.* [6], where the production cross-section distribution of Ir-element isotopes (also corresponding to a two-proton-removal process) coming from the reaction 800-MeV/u ^{197}Au+p [6] was compared with that from the reaction 1000-MeV/u ^{197}Au+Al [3], and the production cross-section distribution of the Ir isotopes from 800-MeV/u ^{197}Au+p was also more neutron-deficient than that from 1000-MeV/u ^{197}Au+Al (see Fig. 7 of Ref. [6]). The authors interpreted this fact in terms of a higher excitation energy deposited in the prefragment by the cascade of nucleon-nucleon collisions induced by one single proton, leading to more neutrons evaporating. This case was attributed to very different geometrical conditions between the proton- and heavy-ion-induced reactions, meaning that the proton needs to react with the gold nucleus in a more central collision to remove two protons, while a loss of only two protons in a heavy-ion-induced reaction can be obtained only in very peripheral nuclear collisions [6]. The discussions above seem to be reasonable, and may be used to explain the results shown in Fig. 3(a) and Fig. 3(b).

For neutron-rich Hg isotopes the experimental data are not sufficient to discuss in detail the production mechanism of neutron-rich heavy residues. For the present reaction 600-MeV ^{18}O+^{nat}Pb, the production cross sections for neutron-rich Hg isotopes, i.e., $^{203,205-209}$Hg, seem to have a typical Q_{gg} dependence that is similar to that discovered for the deep-inelastic collision process [21] as discussed in Ref. [15]. The production mechanism of neutron-rich heavy residues in a relativistic heavy-ion collision has been attributed to cold fragmentation, and an analytical description of the cold-fragmentation process has been used to reproduce the production cross sections of the neutron-rich heavy residues from the reaction ^{197}Au+Be at 950 MeV [7]. For the little peak region shown in Fig. 3(b), the production cross sections of the neutron-rich Hg isotopes from relativistic heavy-ion nuclear reactions are five to nine times higher than those from intermediate-energy heavy-ion nuclear reactions, implying that an additional mechanism contributed to the production of the neutron-rich Hg isotopes just below the heavy-projectile/target mass in the relativistic energy range. The contribution from the additional mechanism depends on the size and neutron-to-proton ratio (N/Z) of the other partner (the lighter nucleus of the projectile and target here). This additional reaction mechanism would preferably be a quick and direct peripheral interaction process such as direct nucleon ablation, few-nucleon transfer, or a nucleon exchange process. However, this quick and direct nuclear interaction process can cover only a very narrow mass region below the mass number of the heavy partner. If a neutron-rich nucleus can be produced only by adding some neutrons in the heavy nucleus, the additional mechanism will stop working, and the production cross sections of the neutron-rich heavy residues will not stay much higher than the corresponding cross sections for intermediate-energy heavy-ion reactions.

V. SUMMARY

For the radioactive Hg isotopes produced in the 600-MeV $^{18}O + ^{nat}Pb$ reaction, complete measurements of independent cross sections have been made using a gamma-ray spectroscopic technique coupled with fast gas thermochromatography. We successfully measured the production cross section down to about 2 μb. The present experimental Hg-isotope distribution was compared with those from previously reported production of Hg isotopes from 1-GeV/u ^{208}Pb–induced reactions on protons [8,9], deuterons [10], and copper [11], and from 600-MeV protons on natural lead targets [18]. These comparisons showed a huge increase in the yields of neutron-deficient heavy residues with increased projectile energy from intermediate energy to relativistic energy, implying a huge increase of the fast-neutron yields emitted instantaneously in the reaction process. At the same time, it was confirmed that relativistic-energy proton-induced reactions are preferable to other reactions induced by heavy-ion projectiles in a spallation neutron source if the effective bombarding energy of the protons is set in the energy range from 1 GeV to 600 MeV. For proton-induced reactions at relativistic energies the more neutron-deficient heavy residues, related to two-proton-removal or similar processes, may be produced in more central collisions, in agreement with the results obtained in Ref. [6]. On the other hand, the heavy-ion-beam-induced reactions provide an effective tool for producing new neutron-rich isotopes in the heavy neutron-rich region.

ACKNOWLEDGMENTS

We would like to thank the staff of the HIRFL national laboratory, especially those of the accelerator section for the excellent operation of the machine. We would also like to thank Professor T. T. Inamura for repeated critical reading of our manuscript. This work was supported by the National Natural Science Foundation of China under Grant Nos. 19975058 and 19575065.

[1] *International Conference on Accelerator-Driven Transmutation Technologies and Applications*, edited by E. D. Arthur, A. Rodriguez, and S. O. Schriber, AIP Conf. Proc. No. 346 (AIP, Woodbury, NY, 1995).

[2] J. M. Carpenter, Nucl. Instrum. Methods **145**, 91 (1977).

[3] K.-H. Schmidt, T. Brohm, H.-G Clerc, M. Dornik, M. Fauerbach, H. Geissel, A. Grewe, E. Hanelt, A. Junghans, A. Magel, W. Morawek, G. Münzemberg, F. Nickel, M. Pfützner, C. Scheidenberger, K. Sümmerer, D. Vieira, B. Voss, and C. Ziegler, Phys. Lett. B **300**, 313 (1993).

[4] K.-H. Schmidt, K. Sümmerer, H. Geissel, G. Münzemberg, F. Nickel, M. Pfützner, M. Weber, B. Voss, T. Brohm, H.-G Clerc, M. Fauerbach, J. J. Gaimard, A. Grewe, E. Hanelt, M. Steiner, J. Weckenmann, and C. Ziegler, Nucl. Phys. **A542**, 699 (1992).

[5] M. de Jong, K.-H. Schmidt, B. Blank, C. Böckstiegel, T. Borhm, H.-G. Clere, S. Czajkowski, D. Mornik, H. Geissel, A. Grewe, E. Hanelt, A. Heinz, H. Irnich, A. R. Junghang, A. Magel, G. Münzenberg, F. Nickel, M. Pfützner, A. Piechaczek, C. Scheidenberger, W. Schwab, S. Steinhäuser, K. Sümmrrer, W. Trinder, B. Voss, and C. Ziegler, Nucl. Phys. **A628**, 479 (1998).

[6] J. Benlliure, P. Ambruster, M. Bernas, A. Boadard, J. P. Dufour, T. Enqvist, R. Legrain, S. Leray, B. Mustapha, F. Rejmund, K.-H. Schmidt, C. Stéphan, L. Tassan-Got, and C. Volant, Nucl. Phys. **A683**, 513 (2001).

[7] J. Benlliure, K.-H. Schmidt, D. Dortina-Gil, T. Enqvist, F. Farget, A. Heinz, A. R. Junghans, J. Pereira, and J. Taieb, Nucl. Phys. **A660**, 87 (1999).

[8] W. Wlazlo, T. Enqvist, P. Armbruster, J. Benlliure, M. Bernas, A. Boudard, S. Czájkowski, R. Legrain, S. Leray, B. Mustapha, M. Pravikoff, F. Rejmund, K.-H. Schmidt, C. Stéphan, J. Taieb, L. Tassan-Got, and C. Volant, Phys. Rev. Lett. **84**, 5736 (2000).

[9] T. Enqvist, W. Wlazło, P. Armbruster, J. Benlliure, M. Bernas, A. Boudard, S. Czájkowski, R. Legrain, S. Leray, B. Mustapha, M. Pravikoff, F. Rejmund, K.-H. Schmidt, C. Stéphan, J. Taieb, L. Tassan-Got, and C. Volant, Nucl. Phys. **A686**, 481 (2001).

[10] T. Enqvist, P. Armbruster, J. Benlliure, M. Bernas, A. Boudard, S. Czajkowski, R. Legrain, S. Leray, B. Mustapha, M. Pravikoff, F. Rejmund, K.-H. Schmidt, C. Stéphan, J. Taieb, L. Tassan-Got, F. Vivés, C. Volant, and W. Wlało, Nucl. Phys. **A703**, 435 (2002).

[11] H. Geissel, P. Armbruster, K. H. Bchr, A. Brünle, K. Burkard, M. Chen, H. Folger, B. Franczak, H. Keller, O. Klepper, B. Langenbeck, F. Nikel, E. Pfeng, M. Pfützner, E. Roeckl, K. Rykaczewski, I. Schardt, C. Scheidenberger, K.-H. Schmidt, A. Schröter, T. Schwab, K. Sümmerer, M. Weber, G. Münzenberg, T. Brohm, H.-G Clerc, M. Faucrbach, J.-J. Gaimard, A. Grewe, E. Hanelt, B. Knödler, M. Steiner, B. Voss, J. Weckenmann, C. Ziegler, A. Magel, H. Wollnik, J. P. Dufour, Y. Fujita, D. J. Vieira, and B. Sherrill, Nucl. Instrum. Methods Phys. Res. B **70** 286 (1992).

[12] K. Sümmerer, W. Brüchle, D. J. Morrissey, M. Schädel, B. Szweryn, and Yang Weifan, Phys. Rev. C **42**, 2546 (1990).

[13] R. Yanez, W. Loveland, K. Aleklet, A. Srivastava, and J. O. Liljenzin, Phys. Rev. C **52**, 203 (1995).

[14] D. W. Bardayan, M. T. F. da Cruz, M. M. Hindi, A. F. Barghouty, Y. D. Chan, A. Garcia, R. M. Larimer, K. T. Lesko, E. B. Norman, D. F. Rossi, F. E. Wierfeldt, and I. Zlimen, Phys. Rev. C **55**, 820 (1997).

[15] Zhang Li, Zhao Jinhua, Zheng Jiwen, Wang Jicheng, Qin Zhi, Yang Yongfeng, Zhang Chun, Jin Genming, Guo Guanghui, Du Yifei, Guo Tianrui, Wang Tongqing, Guo Bin, and Luo Yixiao, Phys. Rev. C **58**, 156 (1998).

[16] Zhao Jinhua, Zhang Li, and Zheng Jiwen, At. Energy Sci. Technol. **31**, 530 (1997) (in Chinese).

[17] Zhang Li, Wang Jicheng, Zhao Jinhua, Yang Yongfeng, Zheng Jiwen, Qin Zhi, Zhang Chun, and Guo Tianrei, High Energy Phys. Nucl. Phys. **21**, 156 (1997) (in Chinese).
[18] J. W. Zheng, L. Zhang, J. H. Zhao, and Q. Y. Hu, J. Nucl. Radiochem. **21**, 1 (1999) (in Chinese).
[19] V. Reys and W. Westmeier, At. Data Nucl. Data Tables **29**, 1 (1983).
[20] B. Jonson, O. B. Nielsen, L. Westgard, and J. Zylicz, CERN Report No. 81–09, 1981, 640–643.
[21] V. V. Volkov, Phys. Rep. **44**, 93 (1978).